CHALMERS

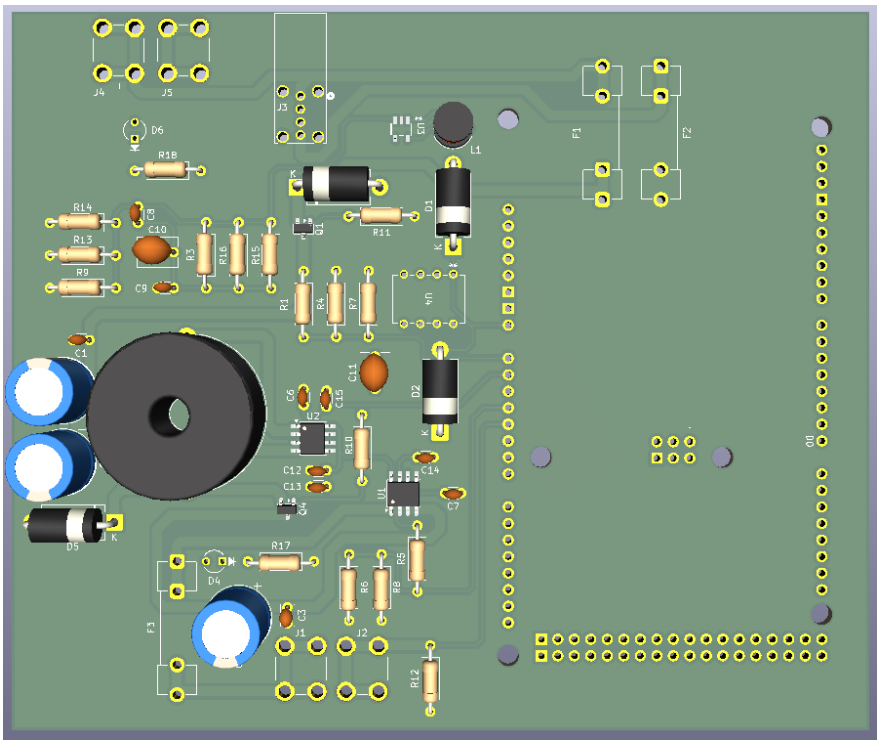

Solar-fed Portable Charging Module for Camping

Bachelors thesis report in Electrical Engineering

Oliver Sandström, Gabriel Moberg, Anton Hasselgren and Simon Karlsson

DEPARTMENT OF ELECTRICAL ENGENEERING

CHALMERS UNIVERSITY OF TECHNOLOGY

Gothenburg, Sweden 2026

www.chalmers.se

Bachelors thesis report 2026

Solar-fed Portable Charging Module for Camping

Oliver Sandström
Gabriel Moberg
Anton Hasselgren
Simon Karlsson

CHALMERS

Department of Electrical Engineering
Chalmers University of Technology
Gothenburg, Sweden 2026

Solar-fed Portable Charging Module for Camping
Oliver Sandström, Gabriel Moberg, Anton Hasselgren & Simon Karlsson,

Supervisor: Vaishnavi Ravi, Department of Electrical Engineering
Examiner: Jimmy Ehnberg, Department of Electrical Engineering

Degree project report 2026
Department of Electrical Engineering
Chalmers University of Technology
SE-412 96 Gothenburg
Sweden
Telephone +46 31 772 1000

Cover: Prototype circuit board featuring DC - DC converter module with MPPT for camping

Typeset in LaTeX
Gothenburg, Sweden 2026

Abstract

With an increasing interest in outdoor recreational activities such as hiking and camping and an increasing reliance on portable gadgets, the demand for portable power solutions is expanding. This project aims to design and prototype a solar fed portable charging module to address such a demand.

The aim of the project is to efficiently extract solar energy and support charging of a power bank. The system architecture consist of an input from a solar panel, the designed DC-DC converter and a power bank as energy storage source. To efficiently extract solar energy, a Perturb & Observe based Maximum Power Point Tracking algorithm, along with the suitable charging control logic is implemented. The DC-DC converter and the control algorithm is verified using MATLAB Simulink. Following the simulation, a hardware prototype PCB is designed using KiCad with the control logic implemented on the Arduino platform.

While the basic functionality of hardware is tested, further testing of the DC-DC converter with the implemented control logic needs to be performed in the future.

Key Words: DC-DC converter, MPPT, Solar, Battery Bank, Charging.

Acknowledgements

We would like to extend a big thank you to our supervisor Vaishnavi Ravi and our examiner Jimmy Ehnberg for their guidance during this project. We would also like to thank C.A.S.E lab for allowing us to use their lab.

List of Acronyms

Below is the list of acronyms that have been used throughout this thesis listed in alphabetical order:

BMS	Battery Management System
CC	Constant Current
CV	Constant Voltage
IC	Integrated Circuit
I/O	Input/Output
I-V	Current-Voltage
MCU	Microcontroller Unit
MPP	Maximum Power Point
MPPT	Maximum Power Point Tracking
PCB	Printed Circuit Board
PI	Proportional-Integral
P&O	Perturb and Observe
PV	Photovoltaic
P-V	Power-Voltage
PWM	Pulse-Width Modulation
SIMO	Single Input, Multiple Output

Contents

1

Introduction

1.1 Background

Outdoor activities such as camping and hiking are on the rise in the USA and Europe, with a sharp increase in recent years following the covid-19 pandemic [1] [2]. Such rising interest in outdoor activities also come with an increasing reliance on electronic devices such as smart phones, GPS navigators, speakers and lamps used for essential functions and entertainment purposes. This growth creates a demand and market for portable charging modules that can power the electronic devices brought along during the outdoor activities.

Employing renewable energy sources to power the electronic devices is a cleaner, environmentally friendly and sustainable solution. It is also better suited for implementation in portable small scale applications due to its modularity and resource-independency, as compared to fossil fuel solutions [3]. This makes renewable energy solutions both a more marketable and more effective alternative for portable charging modules.

One of the renewable energy sources that is widely used to generate electricity is solar energy. Solar energy conversion accounts for 7% of the electricity produced globally [4]. Solar panels are commonly made up of arrays of photovoltaic cells that convert this solar energy into electrical energy.

Among the commonly employed renewable energy sources such as wind energy, hydro power and bio energy, solar energy generation is often more practical and advantageous in terms of portability, modularity and ease of setup [3]. It is also silent compared to other energy solutions, such as wind turbines which often lead to local noise pollution, and has a good longevity as well as a low maintenance cost [5] [6] . The advancement of photovoltaic cell research has also resulted in the development of light, thin and flexible foldable panels which furthermore make PV arrays a promising choice for applications in hiking and camping scenarios [7].

However there are a few challenges that need to be addressed when utilizing photovoltaic solar panels. Due to their semiconductor structure they exhibit a non linear electrical characteristic [8]. This can be shown in the I-V characteristics of solar panels, where it can be seen that the panels can provide constant voltage over a range of operating currents, up until the curves knee point. Near this point the panel operates at its MPP, where the maximal amount of power is extracted by the cells. Beyond this point where the curves knee point is reached, small increases in current result in drastic decrease in voltage, leading to a collapse of the power output. The non linear I-V characteristics of the PV panels and their MPP is also sensitive to environmental conditions such as temperature and irradiance [8]. Therefore a suitable control system, a MPPT system, is required in applications utilizing PV panels, to avoid the panels moving away from their optimal operating point, MPP, which would result in poor energy extraction and less power provided to the application, making it less efficient.

Another challenge that arises with solar energy sources is their dependency on weather and time of day, there is a need for energy storage capabilities [9]. A common way to solve this problem is to integrate a battery that will allow for storage of energy during periods of excess power generation and that can then be utilized as a supplement or replacement during poor energy production conditions, such as nighttime and cloudy weather.

Among the available energy storage solutions, lithium ion batteries are widely used in portable applications due to their low weight, high energy density, long life cycle and relatively low self-discharge rate [10]. However, lithium ion batteries are sensitive to over-charging, deep discharge and thermal stress. Therefore a BMS is required to ensure safe charging of the batteries [11]. Further lithium ion batteries have different charging states, constant current state and a constant voltage state, for which the charging must be regulated [9]. A DC-DC converter can be used in combination with control logic in order to regulate the electrical parameters to ensure they are adapted to these states.

1.2 Purpose and Objectives

The purpose of the project is to design and build a prototype of a solar powered charging module that is both able to extract maximum energy from the solar panel, thus increasing efficiency, and has integrated power storage capabilities, ensuring a more dependable charging ability.

The following objectives, as listed below are formulated to achieve the purpose of the project:

1. Design and dimension a DC-DC converter in the module to meet the charging

requirements of the battery.

2. Design and implement a hardware prototype of the module.

3. Implement a MPPT method that will ensure maximum energy extraction from the PV array

4. Implement the charging control profile with a constant current and constant voltage mode to ensure safe and efficient charging.

1.3 Scope

The aim of this project is to demonstrate the feasibility of the concept and to produce a working prototype. This means many features that would be expected of a consumer-ready product will not be implemented. The following points are considered beyond the scope of this project.

1. While the project initially aimed in implementing a multi output converter for multiple loads, the current scope of the project is restricted to demonstrating the charging of a battery bank from the PV source due to time constraints.

2. The built hardware prototype is tested with a commercial power bank purchased, in place of the standard lithium ion battery to ensure a safe initial testing environment.

2

Technical Background

In this chapter, the technical aspects of the main components involved in the project are discussed. Figure 2.1 presents the block diagram of the proposed system.

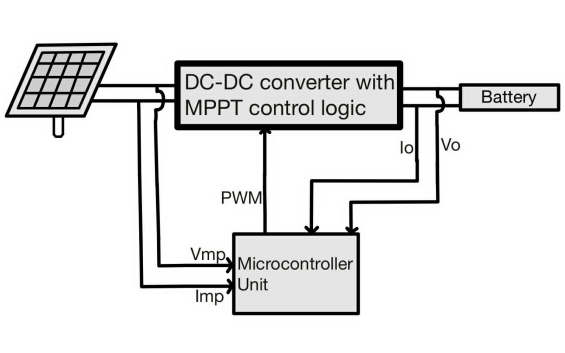

Figure 2.1: Block Diagram representation of solar fed battery charging circuit

2.1 Photovoltaic Array

Photovoltaic systems are renewable energy solutions that harness solar power to generate electricity. Solar cells are the fundamental components of photovoltaic systems, which are responsible for the conversion of solar energy into electricity [12]. They utilize p-n junction semiconductors and work on the principle of the photoelectric effect. When the cell is hit by photons from the sun, with energy exceeding the semiconductor bandgap, the electrons in the conduction band are ejected and electron hole pairs are created on both sides of the junction. These charges are diffused over the junction and are accelerated in opposite directions due to the junctions internal electrical field, creating an electric current.

2.2 Maximum Power Point Tracking

The behavior of a PV array is generally depicted in terms of the I-V and P-V characteristics. These are dependent on temperature and irradiance. Figure 2.2 presents the I-V

and P-V characteristics of a PV array at temperatures of 25 °C and 45 °C respectively with a irradiance of 1000 W/m^2.

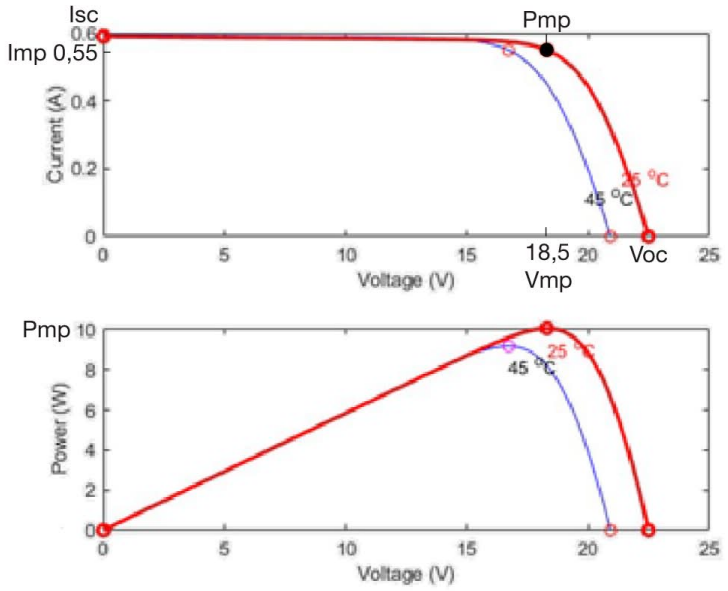

Figure 2.2: Photovoltaic Array Characteristics. Generated using MATLAB Simulink.

Due to the semiconductor structure of the photovoltaic cells, the PV array exhibits non linear electrical characteristic, which is demonstrated by the graphs as shown in figure 2.2. The PV panels exhibit a constant current characteristic until reaching a specific voltage threshold [8]. Beyond this point the current rapidly declines as the voltage increases. This transition is called the knee point and near this point lies the maximum power point of the solar panel. The maximum power point is depicted by the red and blue circle in the curve corresponding to 25 °C and 45 °C respectively. It is important to operate the solar panels at this point to ensure maximum power extraction. To achieve this, a suitable MPPT algorithm is implemented in the controller, which controls the operating duty cycle of the DC-DC converter which regulates the power flow between the solar panel to load.

There are different methods employed to achieve MPPT. Some of the methods commonly used are P&O, Incremental conductance, Fractional open circuit voltage, Fuzzy logic control, Particle Swarm Optimization methods etc. Among the MPPT methods, P&O is the simplest and easiest to implement and is widely employed to perform maximum power point tracking [13]. The approach is showcased in figure 2.3.

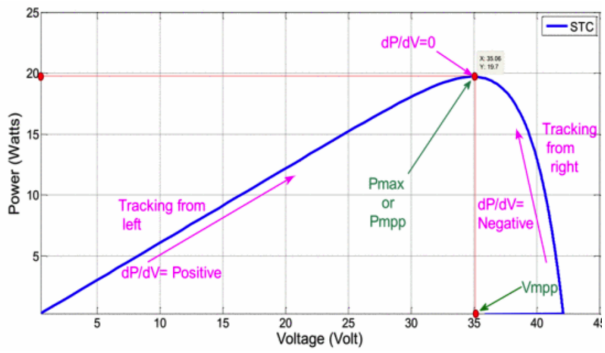

Figure 2.3: Power Voltage Characteristic of Solar panel with the P&O MPPT method [14] © [2017] IEEE.

In this method, the controller adjusts the operating voltage of the array by a small increment (dV) and measures the power delivered by the PV panel. If the power delivered is increased in comparison to the previous power (i.e. dP/dV is positive), then the controller continues to adjust the operating voltage of the array in the same direction, until the power no longer increases, i.e. $dP/dV = 0$. This points corresponds to the MPP of the PV curve. The method is called perturb and observe, since it involves adjusting the operating voltage and observing the corresponding changes in power. If the power increases ($dP/dV > 0$), the algorithm continues to increase in the same direction, otherwise if $dP/dV < 0$, the algorithm reverses the direction of perturbation.

2.3 DC-DC Converter

In a photovoltaic system, a DC-DC converter serves as an important interface between the PV source and the load. DC-DC converters are commonly employed to convert and regulate the voltage / current at the source to meet the load requirements [15]. The output is regulated by involving switching of one or more transistors usually MOSFETs. The switching of the MOSFETs is controlled by adjusting the switch ON and OFF duration (T_{on} and T_{off}), using a PWM signal.

2.3.1 Buck Converter

One basic topology of DC-DC converters is the buck converter. It is a step down converter, which produces a lower output voltage compared to the input voltage [15]. The basic electrical schematic for a buck converter, with a MOSFET as switch is presented in figure 2.4.

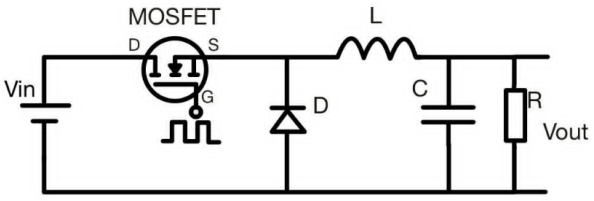

Figure 2.4: Circuit Diagram of Buck Converter

The input - output voltage relation in a buck converter is given by

$$V_{out} = D \cdot V_{in} \tag{2.1}$$

where D is the duty cycle for the switch [15]. If power losses are neglected making input power equal output power, input - output current relation is given by

$$I_{out} = \frac{I_{in}}{D} \tag{2.2}$$

2.3.2 Boost Converter

The other basic topology of DC-DC converters is the boost converter. It is a step up converter that transforms a lower input voltage to a higher output voltage [15]. The basic electrical schematic for a boost converter, with a MOSFET as switch, can be seen in figure 2.5.

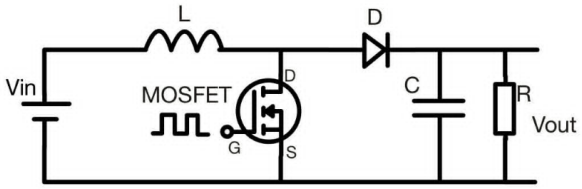

Figure 2.5: Circuit Diagram of Boost Converter

The boost-converter alters the output voltage according to the equation

$$V_{out} = \frac{V_{in}}{1 - D} \tag{2.3}$$

where D is the duty cycle for the switch [15]. Assuming no power losses, the input output

current in the boost converter is given by

$$I_{out} = I_{in} \cdot (1 - D) \tag{2.4}$$

2.4 MOSFETs

In switched mode power converters, the switching element plays a critical role in transfer of energy from source to load [16]. Typically MOSFETs are used as switching elements in DC-DC converters because of their fast switching ability and low conduction losses [17].

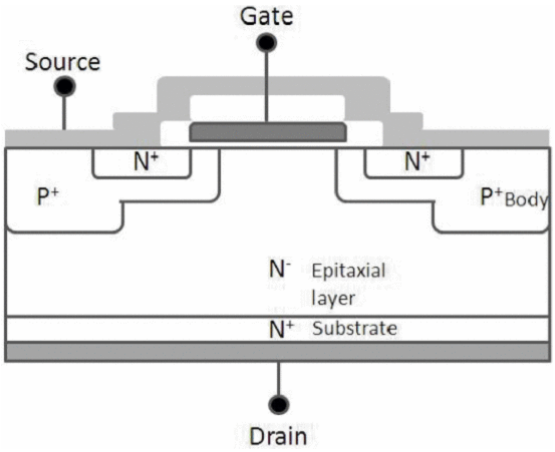

Figure 2.6: MOSFET structure [16] © [2015] IEEE.

A MOSFET is a semiconductor device with three terminals consisting of gate, drain and source as shown in figure 2.6. It has an operating behavior that can generally be divided into three region: cutoff, saturation, and the resistive region [18]. In the cutoff region, the device ideally conducts no drain current. In the saturation region, the drain current is mainly controlled by the gate to source voltage which allows the MOSFET to be modeled as a voltage-controlled current source. The resistive stage the device behaves more like a voltage-controlled resistance between drain and source. This property makes the MOSFET able to work as an electrical switch, since the gate voltage can be used to control the on or off state.

2.5 Controllers

Controllers are used to regulate the behavior of a machine or a system. One type of controller is called MCUs which is widely used for embedded control of different processes in equipments [19]. Furthermore MCUs are considered programmable controllers even if they are not used on an industrial level like other types of controllers. The major key

advantage that makes MCUs suitable for smaller embedded systems is their input/output configuration which are located on a single chip which allows the MCU to be a stand-alone send/receive system suitable for applications such as simpler electronic converter systems or control systems.

For smaller prototype projects with low to medium complexity in control logic, a good choice of MCU is an Arduino because of their easy-to-use interface making the user experience simple and accessible [20]. An Arduino is an MCU with both hardware boards of which could be ordered but also a software that is an open-source electronic platform. To adapt a system to the functions intended by sending instructions from the board, there are two ways to make an Arduino send those instructions. One way is to use the Arduino programming language based on the wiring of the board and the other way is to use the Arduino software (Arduino IDE) which is based on programming with C++ instead of the wiring of the first method [20].

One method for controlling the switching of MOSFETs in DC-DC converters is PWM. This method employs switching at a constant frequency, making a constant switching time period $T_s = T_{on} + T_{off}$, and regulating the on duration of the MOSFET, the duty cycle, in order to control the output voltage [15].

The switch control signal that controls the state of the switch, is generated by comparing a signal level control voltage v-control with a repetitive sawtooth waveform. When the V_{so} exceeds the v-control the switch control signal demands the PWM signal to turn on and vice versa. Usually the control voltage is taken from an amplified error, or by calculating the difference from the output and a theoretical reference. In figure 2.7 this can be seen.

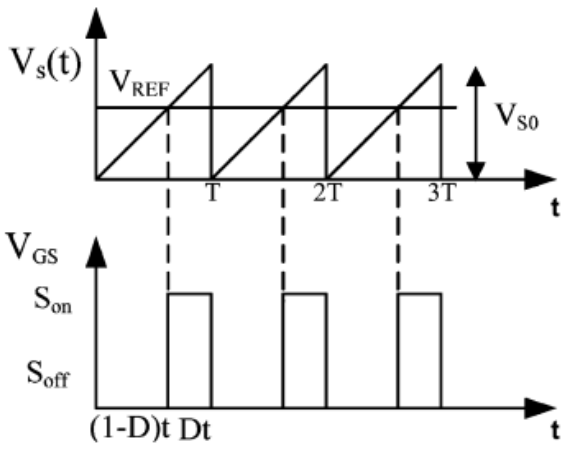

Figure 2.7: Pulse width modulation [21] © [2007] IEEE.

There are several advantages to using PWM techniques. Firstly they are easy to implement

and control. Secondly they lead to a lower power dissipation and reduce the amount of lower order harmonics [22]. For converters and inverters, a well selected PWM signal leads to reduced current ripple [23]. This can also be seen in the formula for current ripple in a buck converter

$$\Delta I_L = \frac{\left(V_{\mathrm{IN(max)}} - V_{\mathrm{OUT}}\right) D}{f_S \cdot L}$$

which shows how the Inductor ripple current improves with a higher choice of switching frequency [24].

2.6 USB

USB is a widely adopted connector standard designed to handle both data transfer and power delivery through a single port [25]. These USB connectors can be distinguished in two different ways, connector shape and version. The letter denotes the shape of the connector and the number denotes which version and thereby the transfer speed and current levels.

USB type A 2.0 contains the following pins:

- V_{BUS}: The power carrying channel that provides voltage and from which the connected device can draw current.
- GND: Return channel for the signal.
- D+ and D-: The data pins enable the transfer of data and signaling.

The data pins can be connected to a processor and used to transmit data [26]. If data transfer is not needed, for example in a charger, the data pins can be disconnected, this signals to a connected device that only the standard 500mA can be drawn from the receptacle. If the data pins are shorted to each other, it signals to the device that it is connected to a dedicated charging port, allowing for higher current draw.

2.7 Battery

One of the important components in a solar based battery charging system is the energy storage interface, i.e. the batteries. In general, lithium based batteries are employed due to their high energy density and longer life span. A multi stage charging profile (CC / CV) is required by the battery to ensure efficient energy transfer from the source over the battery's lifespan [9]. Figure 2.8 presents the charging profile of lithium ion battery.

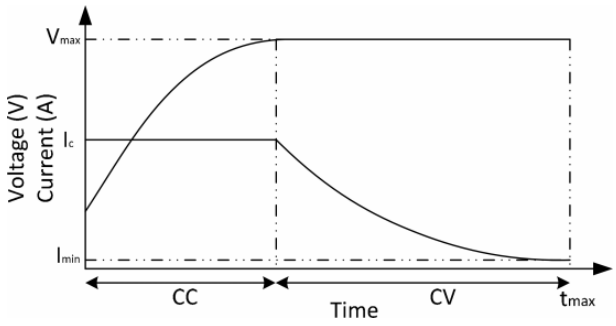

Figure 2.8: CC CV [9] © [2012] IEEE.

The charging process begins with bulk stage (CC), where the controller maintains a maximum steady current, I_{b-max}, while the battery voltage rises to safe transition voltage corresponding to approximately 90% of state of charge (SOC). Then the system operates in the absorption stage, where the current is gradually reduced until it reaches a predefined termination current.

The charging control logic for the battery is implemented using an MCU as discussed in earlier section. The controller drives the converter in current control mode, and adjusts the duty to draw maximum power from the source [27]. At the transition threshold, the controller switches from current control mode to voltage control mode. Furthermore the PI controller implemented on the Arduino, measures the error between the reference voltage and battery voltage, controls the duty cycle to ensure the voltage does not exceed the reference voltage and allows current to gradually lower to the termination value. The transfer function of the PI controller is given by

$$G_c(s) = K_p + \frac{K_i}{s} \tag{2.5}$$

where Kp corresponds to proportional gain and Ki corresponds to integral gain. The proportional and integral gains are tuned to achieve optimal transient and steady state response.

3

Method

This chapter discusses the method involved in the design and implementation of the DC-DC converter for solar fed battery charging.

The complete system is visualized as

1. Input stage, which involves selection of appropriate solar PV array
2. Power stage, which involves selection and design of a suitable converter topology
3. Output stage, selection of suitable battery for camping application
4. Sensing stage which involves the design of current and voltage sensing circuits
5. Control stage, which involves all for the implemented control logic
6. Protection, which includes the different forms of preemptive protection

The following subsections discuss the design and selection method associated with each stage. The figure 3.1 below is an illustration of the whole system with descriptions.

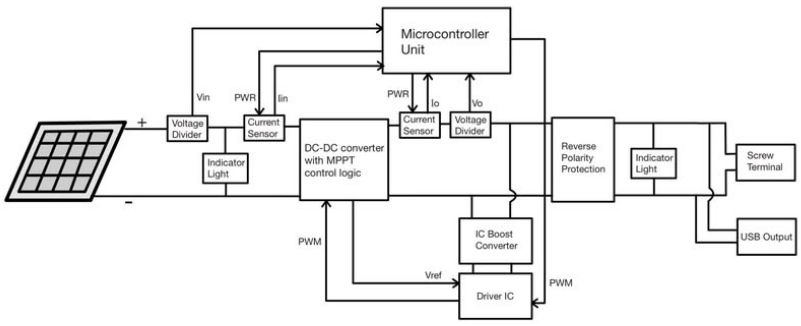

Figure 3.1: Illustration of the System

3.1 Input Stage

As discussed in the previous sections, the input to the converter is from the PV array. The PV array is selected based on certain factors such as power consumption, portability, and the environmental conditions during camping. Since the goal is to provide power to low power loads and a high degree of portability, the load power requirement is considered to be to charge a battery or an equivalent power bank of 10 000 mAh. The power bank had an input voltage of 5 V and maximum input current of 3 A. Therefore as to not exceed the power consumption of the power bank, a PV panel with 15 W output would be ideal. However the closest option that did not exceed maximal consumption was a PV panel with 10 W maximum capacity.

A PV panel with an operating voltage of 18.5 V and 0.55 A at maximum power point was selected for implementation. Though a foldable panel would be a preferred choice, the Seeit 10 W panel is selected considering the cost and availability [28]. It has an open circuit voltage of 22.5 V and a short circuit current of 0.59 A.

3.2 DC-DC Converter

Based on the selected PV array and load dimensions, a buck converter which is simple and provides a lower output voltage and higher output current in comparison with the input is found suitable to implement for the power stage.

3.2.1 Inductor Selection

The inductor in the buck converter is designed such that the inductor current ripple is between 20 to 40 % of the output current. The output current considering the solar PV operating at maximum power point is computed as follows.

The variables already decided are:

$$V_{in} = 18.5V \qquad V_{out} = 5V$$

$$I_{in} = 0.55A \qquad f_s = 50000Hz$$

Combined with the estimated voltage ripple these are the only necessary variables to dimension the rest of the buck converter [24]. The output current could then be calculated by first calculating the maximum duty cycle

$$D = \frac{V_{out}}{V_{in} \cdot \eta} \Rightarrow \frac{5}{18.5 \cdot 0.9} = \frac{5}{16.65} = 0.3003 \tag{3.1}$$

and then using this in the formula for I_{in}.

$$I_o = \frac{I_{in}}{D} \Rightarrow \frac{0.55}{0.3003} = 1.832A \tag{3.2}$$

From equation (3.2) the inductor ripple could be estimated in the following equation.

$$\Delta I_L = (0.2 \text{ to } 0.4) \cdot I_o \Rightarrow 0.3 \text{ selected} \Rightarrow 0.3 \cdot 1.8315 = 0.549A \tag{3.3}$$

Where 0.3 is selected as an estimation. With the switching frequency of the converter considered as 50 kHz and considering the current ripple to be 30 % of the load current, the inductance is calculated as

$$L = \frac{V_{out} \cdot (V_{in} - V_{out})}{\Delta I_L \cdot f_s \cdot V_{in}} = \frac{5 \cdot (18.5 - 5)}{0.550 \cdot 50000 \cdot 18.5} = \frac{67.5}{508000} = 0.133 \cdot 10^{-3} \Rightarrow 133 \cdot 10^{-6}\,\text{H} \tag{3.4}$$

To ensure that the inductor will function properly and the maximum current carried by the inductor is within the saturation current, I_{L-max} is calculated as

$$I_{sw} = \frac{\Delta I_L}{2} + I_o \Rightarrow \frac{0.550}{2} + 1.832 = 2.106A \tag{3.5}$$

The saturation current for the inductor is 4 A, almost twice of I_{L-max}, which means that the maximum inductor current will not enter saturation current levels [29]. This is also within the maximal current rating for the N channel MOSFET, which is 5.7 A.

3.2.2 Switching Elements

The switching elements used in the buck converter is an N-channel MOSFET and a diode. The N-channel MOSFET is primarily selected based on the maximum voltage blocked by and the current carried by the MOSFET. In the design, the largest voltage blocked by the MOSFET is the input voltage, which upon operation corresponds to 22.5 V. Similarly the maximum current carried by the MOSFET is approximately around 0.59 A. Considering safety margins, the N-channel MOSFET A03400, with 30 V and 5.7 A capability is selected for implementation [30].

Similarly the diode is selected such that it blocks the input voltage and carries the average load current. Thus, RS PRO 2545714 is selected for implementation.

3.2.3 Input and Output Capacitor

The input capacitor in the buck converter is primarily selected based on the root mean square value of the input current ripple and input voltage ripple [31]. Considering the maximum input voltage tolerance to be within 5 %, the maximum input voltage ripple could be calculated as

$$\Delta V_{in} = 18.5 \cdot 0.05 = 0.925V \tag{3.6}$$

From this the minimum value of the input capacitance is given by

$$\begin{aligned} C_{in} &\geq \frac{D(1-D)I_o}{\Delta V_{in} \cdot f_s} \\ \Rightarrow C_{in} &\geq 8.32 \cdot 10^{-6}\,\mathrm{F} \end{aligned} \tag{3.7}$$

The rms value of input current is given by

$$I_{\text{in\_RMS\_max}} = I_o \sqrt{D(1-D) + \frac{1}{12}\left(\frac{V_o}{L\, f_s\, I_o}\right)^2 (1-D)^2 D} = 0.837A \tag{3.8}$$

Meanwhile, the maximum output voltage should have a lower tolerance for ripple. The chosen tolerance is therefore only 1% and for the output the voltage is 5 V which makes the maximum output voltage ripple

$$\Delta V_{out} = 5 \cdot 0.01 = 0.05V \tag{3.9}$$

Based on this C_{out} is calculated as

$$C_{out} \geq \frac{\Delta I_L}{8 \cdot f_s \cdot \Delta V_{out}} \Rightarrow C_{out} \geq 27.47 \cdot 10^{-6}\,\mathrm{F} \tag{3.10}$$

C_{in} and C_{out} is the minimum and therefore the real dimension of the capacitors is larger than this and tested both within the simulation and in the prototype.

3.2.4 Driver Circuit

Firstly the driver IC needed to be able to support a high side MOSFET meaning the driver IC needed to provide a gate source voltage greater than the gate source threshold voltage of the MOSFET. It also had to operate below the maximum gate-source voltage allowed for the chosen MOSFET, 12 V. It also needed to be fast enough to effectively charge and discharge the MOSFET gate at pace that would not lead to switching delays and losses.

IR2101 600 V high-side and low-side gate driver IC fit the criteria, however its normal operating point is 15 V, which exceeded the MOSFETs maximum gate-source voltage. This could be fixed by providing a lower voltage to the driver, effectively inhibiting the operating voltage of the driver to be below the MOSFETs maximum allowed value. To confirm that the driver is fast enough to charge the MOSFET gate the charging time is calculated as

$$t \approx \frac{Q_g}{I_{\text{driver}}} \tag{3.11}$$

where t is the switching time, Q_g is the total gate charge and I_{driver} is the current provided by the driver

From the datasheet for the P-channel MOSFET and driver IC, $Q_{g,max} = 7nC$ and $I_{driver,min} = 130$ mA. This gives the calculation

$$t = \frac{7 \times 10^{-9}}{0.13} \approx 5.4 \times 10^{-8}\,\text{s} = 54\,\text{ns} \tag{3.12}$$

which means the driver can switch at an acceptable rate even in the worst case scenario, since it is a lot faster than the systems switching frequency of 50 kHz

3.2.5 Boost regulator IC

The boost regulator IC had to be able to power both the driver IC and the Arduino. In order to do this it would have to be able to boost the voltage from the DC-link from 5 V up to 11 V, which was an acceptable voltage to power both the Arduino and the driver. It would also need to transmit enough current for both components. A good choice for this was determined to be the MIC2296 - High Power Density 1.2 A Boost Regulator [32]. The boost regulator IC had to be dimensioned to regulate the voltage up to the desired 11 V. This step up regulation was determined via the following relationship.

$$R_1 = R_2 \left(\frac{V_{out}}{V_{ref}} - 1 \right) \tag{3.13}$$

For the boost regulator IC, the variables are

$$\begin{aligned} V_{out} &= 11\,\text{V} \\ V_{ref} &= 1.24\,\text{V} \\ R_2 &= 2.7\,\text{k}\Omega \end{aligned}$$

which gives the value of R1 as

$$R_1 = 21.3\,\mathrm{k}\Omega$$

3.3 Output Stage

First the plan of the project was to select a battery with suitable capacity. However, considering the safety and protection, for the testing of the hardware prototype, a power bank of 10 000 mAh is selected, specifically a Nebo power bank with a charge display to monitor the charging, with max 5 V and 3 A charging [33]. The power bank is connected to the hardware prototype through a USB type A port available on the designed PCB.

Originally the plan was to use USB type C which is a modern and widely adopted standard and as such would be useful for supplying power to the power bank, however due to the compact and complex wiring of USB type C the older and simpler, but still ubiquitous USB type A was chosen. Specifically version 2.0 as it only relies on four conductors: two for power delivery (VBUS and GND) and two for data (D+ and D-). This simplifies the PCB layout without limiting performance since the data pins were also shorted to configure the port as a dedicated charging port. Allowing more than 500 mA to be provided.

3.4 Sensing Stage

To implement MPPT and to regulate the current flowing through the battery, it is important to sense the PV panel input current and voltage as well as the output battery current and voltage, the sensing circuits were selected as follows.

3.4.1 Current Sensing

To sense the input and load current in the converter, a current sensor was implemented, the current sensor chosen for this project is from Allegro Microsystems ACS723 series [34]. It is used for the ability to measure and monitor the current throughout the system, specifically before and after the DC-DC converter. The measuring range for the ACS723 is 5 A this being close to the highest current of 3 A, ensuring an accurate reading. Another important factor is the resolution, meaning how much the voltage changes per unit of current. The selected current sensor has a resolution of 400 mV/A giving a high accuracy and relevance when measuring low currents. Moreover the minimum voltage is 4.5 V and maximum voltage is 5.5 V working flawlessly with the stable 5 V being used in this project. However using this sensor close to other electrical noise can influence the signal. A simple and effective method to counter interact this is to introduce capacitors to the filter pin.

3.4.2 Voltage Sensing

The input voltage from the PV array is sensed and scaled to match the analog digital conversion ability of the controller by using resistive voltage dividers. For voltage dividers the relation is described as following [35].

$$V_{out} = V_{in}\frac{R_2}{R_1 + R_2} \tag{3.14}$$

The output voltage is estimated to be 70% of V_{in}. Since the Arduino controller takes a maximum of 5 V and for safety reasons this is estimated with a 30% lower output. For the voltage divider at the PV array this gives

$$V_{in} = 5\,\mathrm{V}, \quad V_{out} = 3.5\,\mathrm{V} \tag{3.15}$$

By expressing the ratio between R_1 and R_2, it can be written as

$$R_1 = 0.43\,R_2 \tag{3.16}$$

R_2 is selected to be $10\,\mathrm{k\Omega}$, which gives the resistances for the first voltage divider as

$$R_1 = 4.3\,\mathrm{k\Omega}, \quad R_2 = 10\,\mathrm{k\Omega} \tag{3.17}$$

For the second voltage divider by the battery, using the same method but with the values, $V_{out} = 3.5\,\mathrm{V}$ and $V_{in} = 18.5\,\mathrm{V}$ with $R_2 = 10\,\mathrm{k\Omega}$, this gives

$$R_1 = 2.2\,\mathrm{k\Omega}, \quad R_2 = 10\,\mathrm{k\Omega} \tag{3.18}$$

3.5 Controller Stage

The Arduino platform of microcontrollers is chosen due to the project groups familiarity with programming them, and the approachable nature of the platform allows for rapid software development, leaving more time for hardware development. The Arduino mega 2560 was chosen in part due to its extensive I/O capability, featuring many analog inputs useful for monitoring voltages and currents, and PWM-enabled pins to control the MOSFET. It also has a large amount of memory, allowing for more memory-intensive operations and a sufficient clock rate for the application. Dedicated hardware timers also

allowed the MOSFET switching to be run in the background so the main CPU can focus on the control logic.

As mentioned in section 3.2.5, a boost regulator IC was added to supply the driver IC, but also to supply the Arduino with power.

3.6 Protection Circuitry

The most important factor when deciding fuses is the break current, furthermore keep in mind the placement, since the current can be different throughout the system. Another factor to attend is ripple, which needs to be accounted for when deciding the operating current. Both of the previous statement pointed towards Legrand 3 A with the maximum current point equaling 3 A. The reason for adding fuses is to protect the system from overcurrent.

The same criteria as the previous N-channel MOSFET applies in a similar manner for the P-channel MOSFET. The highest voltage scenario for the P-channel MOSFET is 5 V and for the current it is 3 A. All this confirming the SQ2351CES P-channel MOSFET is sufficient [36]. This is implemented to protect the circuitry from reverse polarity.

4

Simulation and Hardware Prototype Development

This chapter discusses the aspects associated with Simulation and Hardware prototype development.

4.1 Simulation

It is important to understand the behavior of DC-DC converter circuits and control algorithms involving interactions with the PV array and the battery at different irradiance conditions and state of charge of the battery . The main purpose of simulating is to prove that the theoretical principle of the project is working and to determine what components need to be a part of the module in order for it to function properly. MATLAB Simulink was used to create the simulation model which mostly used components from the specialized power systems library. The model consists of a PV array, a buck converter, a battery, some measurement blocks, and a MATLAB function block used to implement the MPPT algorithm corresponding to the P&O method.

4.1.1 PV Array

The PV array was the first component that was chosen, that emulated the characteristics of the solar panel. This was important because all components of the system had to be compatible with this array in order for the system to function properly. The PV array from the specialized power systems library is shown in fig 4.1 below.

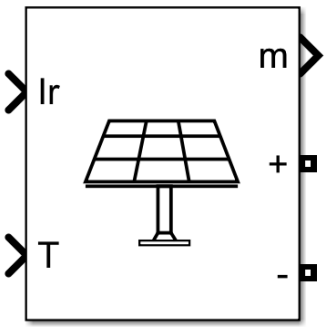

(a) PV array from specialized power systems

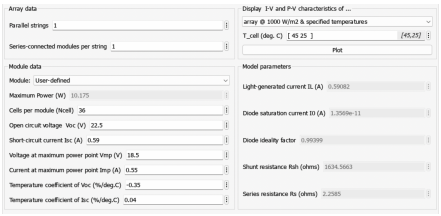

(b) PV array characteristics

Figure 4.1: PV array model and parameters. Taken from MATLAB Simulink.

The PV was matched with characteristics from commercially available photovoltaics systems. The characteristics were therefore set to match with the datasheet of the chosen PV array for this project [28]. Those characteristics taken from the datasheet can be seen in figure 4.1.

Figure 4.1 is the exact implementation of those characteristics but adapted for this specific component block. This was very important for the simulation because otherwise all the dimensioning and measurements would not be giving results of value for this project. Because of this the whole simulation is modeled according to how these characteristics were set.

The P-V and I-V characteristics of the PV array are visualized in figure 4.2 using the plot option in the PV array block, and checked at specified irradiance and temperature.

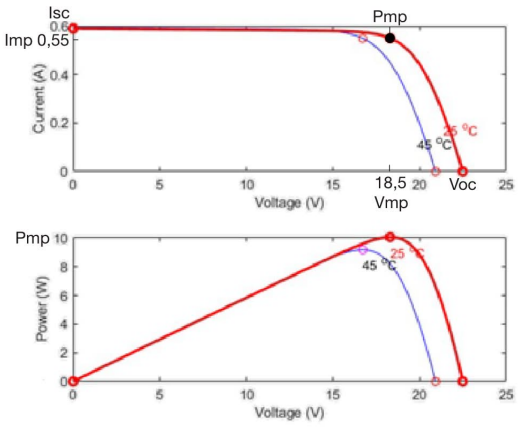

Figure 4.2: Graph characteristics of the PV array. Generated using MATLAB Simulink.

4.1.2 Battery

In order to simulate a load or battery, there were two options that could have been used. One way to simulate this is to use an ideal voltage source that represents a load or the charging of a component. But for this model, the second option was implemented which was to use a battery from the specialized power systems. The battery and its parameters are shown in figure 4.3. The various parameters such as the battery chemistry, nominal voltage and rated capacity are added based on the selected power bank.

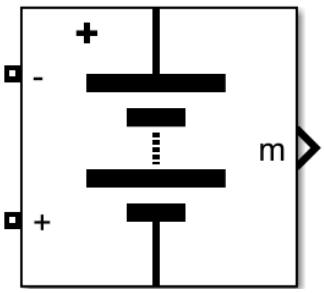

(a) Battery from specialized power systems

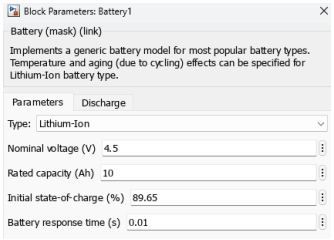

(b) Battery characteristics

Figure 4.3: Battery model and battery parameters. Taken from MATLAB Simulink.

The reason for using this option instead of the ideal voltage source lies within the battery component. When choosing the characteristics for this battery it was rather easy to match it with the power bank chosen. This made the simulation more realistic and easy to implement compared to the other option.

4.1.3 DC-DC Converter

When the PV array and Battery had been selected, a buck converter was constructed and connected to both the PV array and the battery. The buck converter consists of a MOSFET, diode, inductor, and capacitors. These are then connected to a load. This is seen in figure 4.4. The parameters of the various components in the converter are updated based on the calculated values from dimensioning of components discussed in the previous chapter.

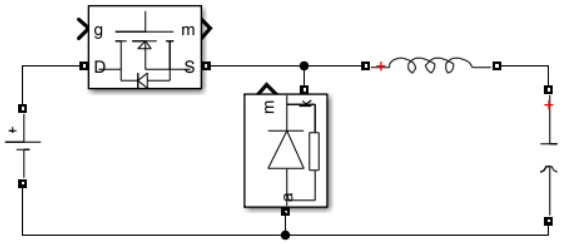

Figure 4.4: Simulation model of buck converter. Generated using MATLAB Simulink.

The MOSFET which could be seen on the top left of figure 4.4 is connected to the PWM generator which receives a duty from the later mentioned MATLAB block in order to switch the MOSFET. After this component there is a diode, followed by an inductor and a capacitor. The buck takes a higher input voltage and lowers it to match with the load of the system. It is with the MOSFET that the whole system is controlled by receiving a specific duty cycle. With the MOSFET the system can adapt to different inputs and arrays in order to operate in the MPP thus making the MOSFET the component which is most important for the system to work according to the characteristics of the PV array. The method implemented for the MOSFET to operate like this is the earlier mentioned P&O method which will be described further in the control algorithm section. The control logic is implemented through the use of a MATLAB function block, seen in figure 4.5

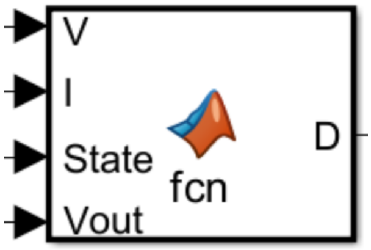

Figure 4.5: MATLAB block with inputs and output. Generated using MATLAB Simulink.

By placing measurement blocks on the input voltage,input current, output current and the state of charge on the battery the MATLAB function receives all input needed for both implementing MPPT and simulating the current drop when the battery is charged to 90% and changes charging state. The MATLAB block then returns the duty cycle for the MOSFET of the buck.

Inside this block the MATLAB code for the control logic lies. The MATLAB block is a theoretical version of the MCU which was used for the hardware prototype.

4.1.4 Model

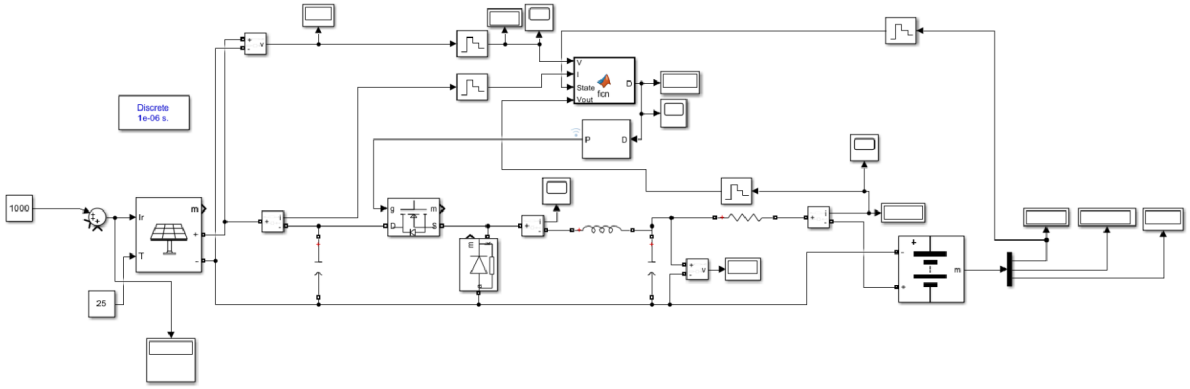

Figure 4.6: The whole simulation model. Generated using MATLAB Simulink.

In figure 4.6 the system is presented as a whole. From the left there is first the PV array. The PV array is the energy source of the system and it gives both the input voltage and input current. The rest of the system is designed to be able to handle the requirements of this component. After the PV array the buck configuration is connected. The buck converter is as previously mentioned, the part which takes the input voltage and input current and lowers it to match with the load. Additionally it is the part which makes the system function to match with the MPP. Therefore the MOSFET could be seen in fig 4.6 being connected to the MATLAB block. From the MATLAB block all the measurements could be seen being connected. Those measurement are:

- **Input voltage**, connected from the pv array output
- **Input current**, connected from the pv array output
- **Output voltage**, connected from after the load
- **Battery state of charge**, connected from after the battery

These are all measurements needed to properly control the MATLAB block and send a duty to the MOSFET.

There could also be seen that the input measurements are connected to a zero-order hold block. This block converts a signal to a discrete time signal with a set sample time. This makes the system more stable by holding a sample for a certain time before then sampling once again. After the buck converter, the chosen load could be seen which is the battery. From this battery there are multiple displays which is important to have so that the output side of the system has readable results. Around the system there are multiple scopes,

those are the best way to see results when simulating as they properly display the oscillation of the system and give a timeline display for when the system operates differently.

The system aims to match with the characteristics of the PV array and these characteristics is set to match with a commercially available real PV array. This was important to have the simulation output results matching as close as possible to a real life scenario and to be able to use results from the simulation to enhance the prototype development. In figure 4.7 the characteristics that the system aims to meet are shown.

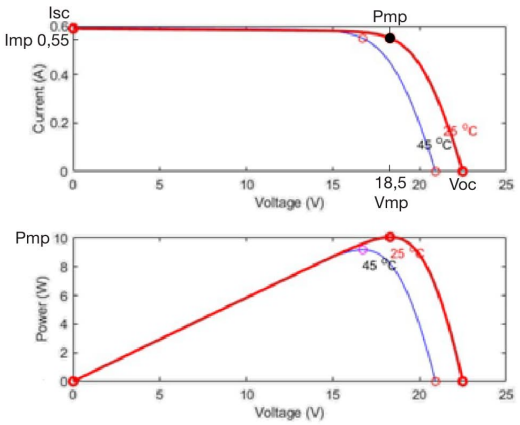

Figure 4.7: Graph characteristics of the PV array. Generated using MATLAB Simulink.

The system as previously mentioned aims to operate in the MPP which could be seen in the graph. For the chosen PV array this is when: V_{in} is equal to 18.5 V and I_{in} is equal to 0.55 A. MPPT is used until the battery reaches 90% state of charge. When this occurs the duty cycle is changed to move the operating power point right on the graph which leads to a higher input voltage but a lower input current. The reason for this is to match the characteristics of the battery which is discussed further in section 2.7 Battery.

4.1.5 Control Algorithm

The code for the P&O method implemented in the code function block was derived from the flowchart presented in figure 4.8 [37].

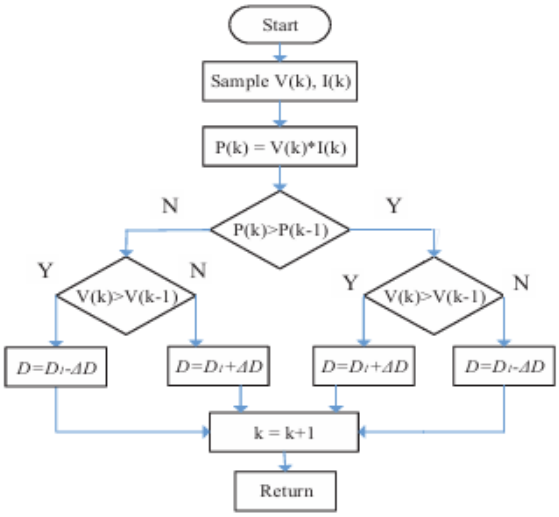

Figure 4.8: P&O MPPT method [37] © [2015] IEEE

Figure 4.8 shows how the duty cycle will get corrected in order to reach the MPP by iterating and comparing previous values to new ones [37]. The method starts with sampling both the input voltage V(k) and the input current I(k). From the input voltage and input current the power is be calculated as

$$P(k) = V(k)\, I(k) \tag{4.1}$$

The calculated power is then compared to previously calculated power which can be seen below

$$P(k) > P(k-1) \tag{4.2}$$

After this the previous voltage is compared to the new voltage

$$V(k) > V(k-1) \tag{4.3}$$

Depending on wether the previously sampled powers and voltages are higher or lower, the duty cycle is changed by either slightly increasing the duty cycle

$$D = D + \Delta D \tag{4.4}$$

or slightly decreasing the duty cycle

$$D = D - \Delta D \tag{4.5}$$

After this the new duty cycle is returned and the simulation iterates once again. This takes place continuously during simulation and is the main principle of the P&O method.

The starting duty in the code is set at 0.5, and the change in duty is set as 0.005. The current at the maximum power point is ensured such that it is within the maximum current limits of the battery. In case this is exceeded, then the current is limited to the maximum charging current of the battery.

When the state of charge of the battery exceeds 90%, the system enters CV mode. In this mode, a PI controller regulates the voltage, and ensures to gradually slow down the charging current. The MATLAB code used for implementation is presented in Appendix. A.

4.2 Hardware Prototype Implementation

The purpose of the prototype is to demonstrate the functionality specifically the MPPT performance and charging efficiency making the portable PV array for camping a reality. The prototype will be the full system (PV array → MPPT converter → power bank) with main focus on the MPPT charging. Heavily based on the Simulink simulation and principles in previous sections this is a physical manifestation on the theoretical solution. The following part will entail the process from the beginning of the design to the final prototype. Starting with inspiration from the simulation with the KiCad schematic, leading into the layout design. Using multiple different methods and materials to create a working prototype with iterative development.

4.2.1 Schematic Design

The PCB was created with KiCad to integrate the solar panel system. Including the different current, voltage sensors and the overcurrent- and reverse polarity protection. The first step is to create a schematic layout that closely resembles the simulation. However since the simulation ends right after the MPPT the rest of the design was made from scratch. Taking the time and iteratively adding components and calculating not only the correct values but also the corresponding size. And using reference points from the different data sheets made this process possible, this was especially handy with more complex components. For example the IC regulator where the needed information regarding the correct use case is presented in the datasheet [32]. However for some scenarios assumptions were necessary and have been selected with safety in mind, which led to adding multiple redundancy component slots and overrating which is a standard power electronics selection practice. The components were selected to follow all our previous results and decisions mentioned earlier in Dimensioning and Component selection. Safety is always a high priority, deciding to use fuses in at least two places to protect the circuit and the people working on it. The first place is right after the input from the PV panel to prevent

unexpected current values directly from the start. Whilst the other fuses are placed towards the end of the system before the charging of the power bank. Where reverse polarity protection was added to protect the circuit from accidental incorrect voltage application.

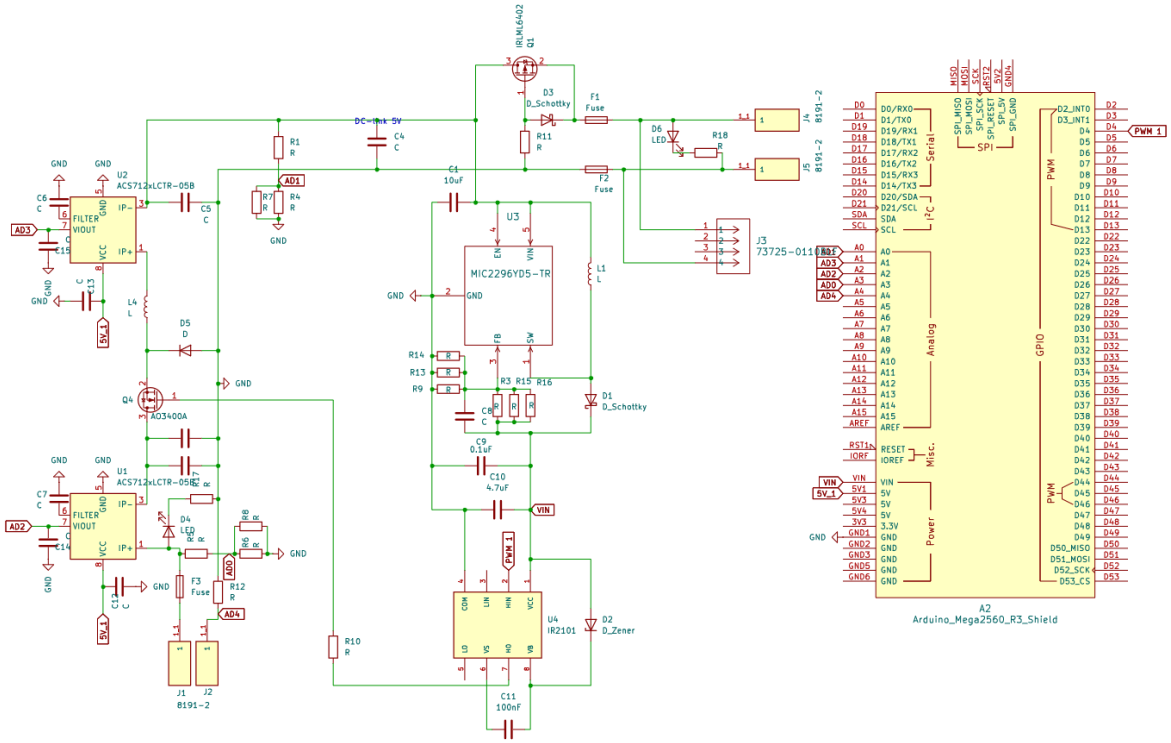

Figure 4.9: Schematic Design. Generated using KiCad.

4.2.2 PCB Layout

The generation of the layout design is simplified by a detailed schematic design. The placement strategy was boils down to placing related components in close proximity to each other, this is more important for the power traces so they do not meet the thermal limitation since they convey higher currents. Another benefit is that it is easier to read the overall circuit when related components are near each other. There are two different trace widths which also played a role in the placements. With the thicker traces corresponding to the power lines and the thinner ones are control lines. With all this in mind there is an infinite amount of different routing options, each with pros and cons.

A compact board matching the Arduino's height is great for improving the manufacturing aspects. Trying to reduce the amount of space the whole PCB takes requires planning and realigning the components to get short and concise paths. This was possible with the use of multiple copper layers, for this design two was used. These were for the traces so that no overlapping occurs, since twice the amounts of connections are possible with the same PCB dimensions. Further extending this concept, with the implementation of a ground

plane on the top layer, this exists for the sole purpose of giving quick and direct access to ground throughout the whole system. Utilizing these layers greatly reduces the length and complexity of the final design. However components close together can introduce electromagnetic noise, to counteract this, careful component placement is necessary. On the other hand heat distribution did not get enough attention, and should have been discussed further. Since this can lead to components not behaving as expected and even in specific cases melt. Honing in on the specific trace width previous mentioned, the maximum current is 3 A meaning a power trace of 1.5 mm will suffice [38].

The biggest challenge was getting all of the connections from the schematic to match and work with the layout. Within this process all of the previous things mentioned needed to be taken into account whilst finding a compromise on compactness for a solution. Another difficult thing to achieve was the surface soldering since the components are so small the room for error is minimal, leading to this part taking more time than anticipated. One more problem that occurred whilst making the PCB was ground plane islands. This term is used to describe a phenomenon where an accidental isolation occurs due to poor trace management. This can lead to charge build ups and arcs, which can disrupt the modules function and leading to an unsafe working environment. The figure 4.10 shown below is the finished layout and the PCB design ordered.

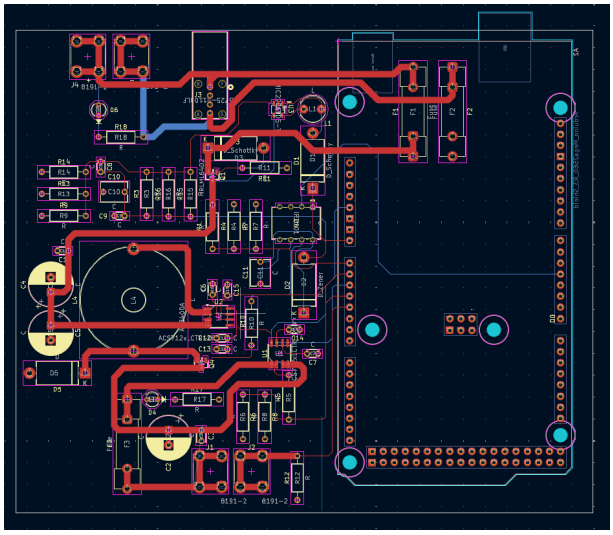

Figure 4.10: Layout Design. Generated using KiCad.

When the PCB and the components had been obtained, they were assembled, mostly by soldering, according to the KiCad layout design. Whilst some problems occurred, studying the datasheet for different components helped in figuring out a workable solution. One major issue that became evident was ground plane islands. In the layout multiple accidental isolated sections were created. Leading to a temporary workaround of adding wires connected directly to places the ground plane was present to parts that were iso-

lated. Following the component placement, multiple parts required to be surface soldered, however the order did not contain a stencil, and there was no access to a soldering furnace. Therefore hand soldering was the only reliable way to get the connections correct, and even with the small footprints it was done with few errors.

4.2.3 Arduino Programming

The first step was to make sure the Arduino could correctly measure the voltage and current in the circuit, and printing them to the console for monitoring purposes. When an analog value is read, the voltage on the pin is converted from a value between 0 and 5 V to an integer between 0 and 1023, to convert this back to a voltage equation (4.6) is used.

$$V_{out} = \frac{ADC_{val} \cdot V_{ref}}{1023} \tag{4.6}$$

In equation (4.6), ADC_{val} is the 10-bit integer from the analog pin and V_{ref} is the system reference voltage (5 V). If the read value originally was a current it must be converted back to a current according to equation (4.7).

$$I_{out} = \frac{V_{in} - V_{offset}}{S} \tag{4.7}$$

In equation (4.7) V_{offset} refers to half of the maximum signal voltage, since the current sensor has a range of -5 to 5 A, meaning 0 A will result in a 2.5 V signal [34]. S refers to the scaling factor of the sensor.

Since the control logic had already been implemented with MATLAB in the Simulink simulations, that code was used as a reference when developing the Arduino control logic programming. The full Arduino code is provided in Appendix. B.

5

Result and Discussion

This chapter discusses the behavior of the designed converter module tested through simulation and hardware testing.

5.1 Simulation Results

In the simulation using the MATLAB model, the charging of the battery is tested in CC mode and CV mode. In CC mode, the working of the converter operating at the MPP is studied. The current flowing through the battery corresponding to MPP is less than the maximum battery current, hence the converter is allowed to operate at the MPP. This was performed with a constant irradiance of 1000 W/m^2, and temperature of 25 °C. The initial duty cycle is set at 0.5 in the code.

Initially the battery state of charge is set at 45% and the converter is tested to verify the P&O algorithm. The duty cycle of the MOSFET is determined based on the implemented P&O code. Figure 5.1 shows the duty cycle changing in response to tracking the MPP from an initial duty cycle of 0.5.

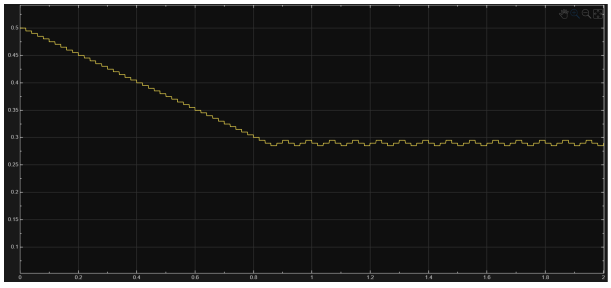

Figure 5.1: Duty cycle from the MPPT controller during the MPPT phase and convergence phase. Generated using MATLAB Simulink.

Up until 0.8 seconds, the controller is in the tracking phase of finding the MPP by adjusting the duty cycle with a fixed step of 0.005, based on the change in power (dP) and voltage

(dV). At around 0.8 seconds, the controller begins to converge and settle around the MPP. There is oscillation around the MPP observed which is characteristic of classical P&O algorithm. The duty cycle reduces as the operating point climbs up towards the MPP with increases in PV power and PV voltage. A dead band is also introduced with no change in duty cycle step when the change in power is within the allowed tolerance. This is added to avoid unwanted hunting around the MPP, which results in undesired oscillations in the inductor current and battery current.

Figure 5.2 and 5.3 show the voltage across the PV array. The MPPT algorithm reduces the duty cycle to move in the direction of increasing input voltage and power towards the MPP. Once the MPP is reached, the duty cycle is retained around the MPP duty cycle and the input voltage settles at around 18.5 V.

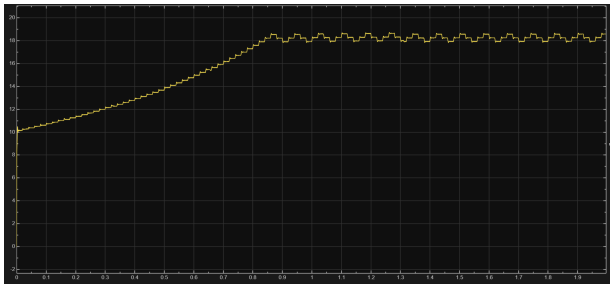

Figure 5.2: Input voltage from the PV array during the MPPT phase and convergence phase

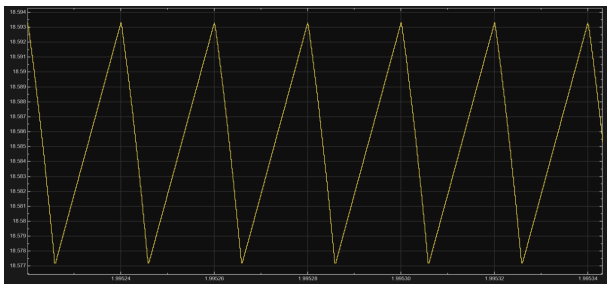

Figure 5.3: Input voltage ripple

Similarly to the voltage, the input current seen in figure 5.4 and 5.5 moves towards the MPP and then settles down at around 0.55 A.

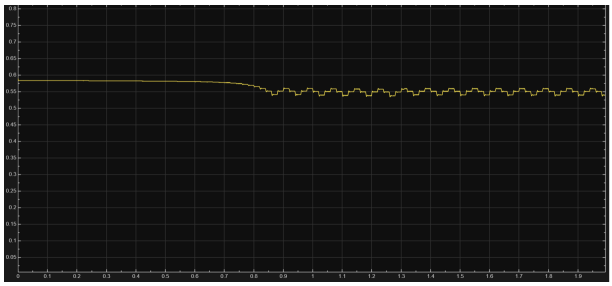

Figure 5.4: PV array current during MPPT tracking and around MPP

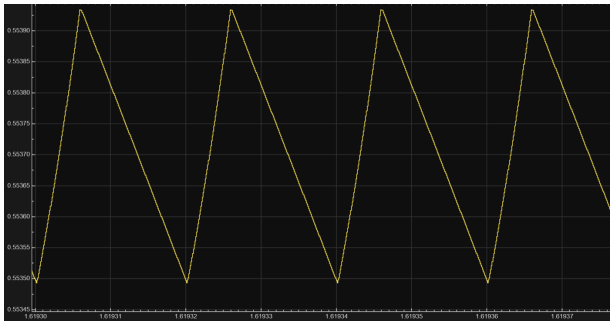

Figure 5.5: Input current ripple

As seen in the previous figures the input voltage and the input current stabilizes at 18.5 V and 0.55 A respectively. This corresponds to the MPP characteristics and means that the PV array extracts maximum power.

Figure 5.6 presents the inductor current. The inductor current has a current ripple of 0.5 A, within 30% of the load current.

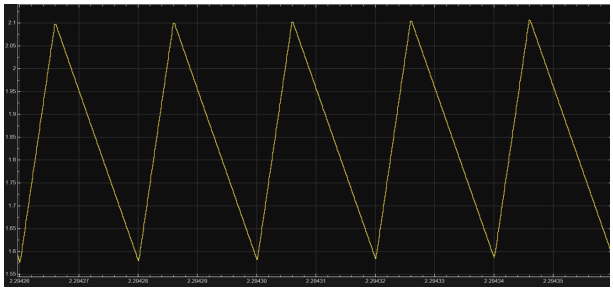

Figure 5.6: Inductor current ripple

Figure 5.7 presents the voltage across the MOSFET. The MOSFET blocks the input voltage when not in conduction. The switching frequency is 50 kHz as defined for PWM and the duty cycle is around 30% corresponding to the conduction period of the MOSFET.

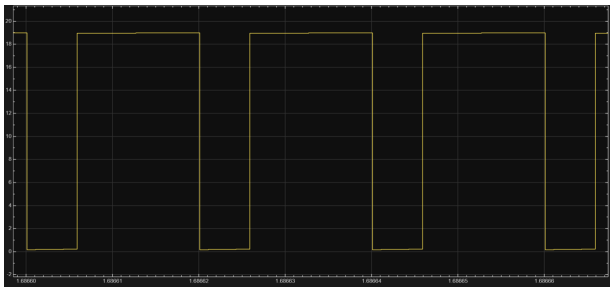

Figure 5.7: Voltage across the MOSFET

Figure 5.8 presents the transition from MPPT and CC mode to CV mode, when the battery charge level has reached 90%. A PI controller gradually reduces the current flowing to the battery. Though the transition occurs at the desired point, the PI controller needs to be further tuned to ensure a better performance.

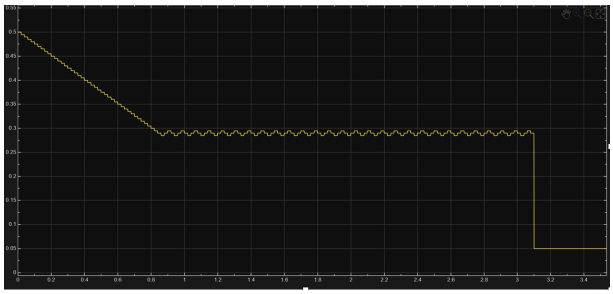

Figure 5.8: MOSFET duty cycle before vs. after transition

From the simulation the functionality of the module has been proven. Control logic for the MOSFET in the converter was implemented which allowed the buck to achieve both MPPT and CC state charging profile. Following the transitioning from MPPT and CC state to CV charging profile was also achieved, however improvements have to be made in the future to get a more stable result.

The time to reach the MPP is 0.8 seconds, which is relatively quick considering the pace of condition changes in the intended environment. However, since the characteristics of the PV panel are known, to decrease the startup time, one could choose a starting duty cycle that would be closer to the desired one, instead of a standard 0.5 starting duty cycle. The change variable for the duty cycle could also be adjusted to allow for larger or smaller changes, affecting the MPPT speed.

Finally the input voltage ripple varied between roughly 18.59 to 18.57 V, which is within the desired 5 % ripple. The input current ripple is varied between roughly 0.5539 to 0.5535 A, which is also very low. The inductor oscillates between 1.56 A and 2.1 A, which is close to the 30% ripple desired.

5.2 Hardware Prototype Results

The primary goal in hardware prototype testing is to verify the basic functionality of the board. To test this, the power board is connected to a low voltage power supply. A simple Arduino code to provide a gate pulse with a switching frequency of 50 kHz and duty cycle of 50% is implemented. The output gate pulse from the controller is verified and the Arduino board is attached to the power board.

The driver circuitry for the MOSFET is powered by the boost regulator IC with input from the output of the converter. However, at first to test the switching performance of the converter, the input from the power bank is bypassed and the boost regulator IC is powered from an additional low voltage power supply. Figure 5.9 presents the output from the driver IC feeding the gate of the MOSFET. The gate pulse is switching at 50 kHz with a duty cycle of 50%.

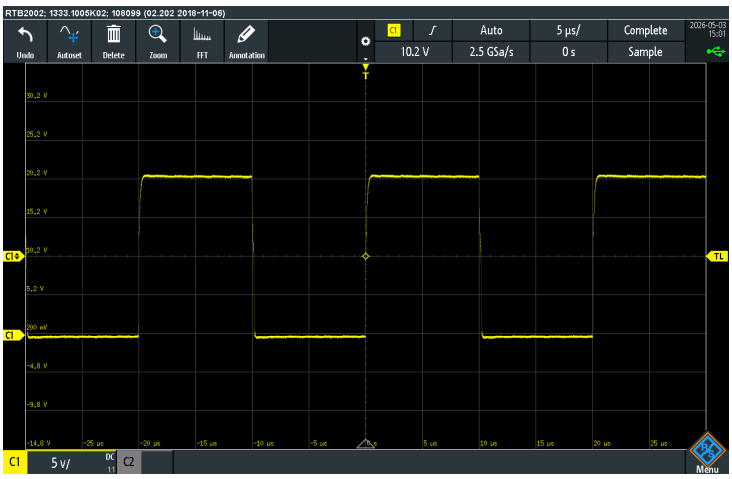

Figure 5.9: MOSFET gate signal from oscilloscope

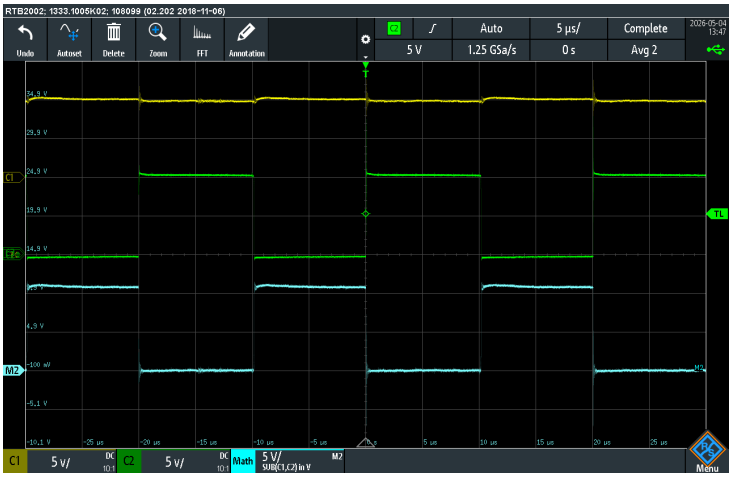

Figure 5.10: Vds taken from oscilloscope

The drain source voltage of the MOSFET is observed to confirm the switching of the MOSFET. Figure 5.10, shows the drain source voltage of the MOSFET. The yellow waveform is the potential at the drain terminal with respect to the ground, and corresponds to the input voltage set at around 10 V, though it is vertically offset and is therefore shows 34.9 V instead of the correct value on the vertical scale. The green waveform depicts the potential of the source pin with respect to ground and is also vertically offset. This also corresponds to the diode voltage of the buck converter. The blue waveform is the drain to source voltage measured through the MATH function (CH1–CH2) in the oscilloscope. The MOSFET blocks the input voltage as expected when the MOSFET is not in conduction.

Following this, it is important to ensure the input voltage and current as well as the output voltage and current are sensed and read properly in the Arduino. The sensed signals from the current sensor and the resistive voltage dividers connected to the analog to digital converter pins of the Arduino are read and displayed at the serial monitor in Arduino IDE. Figure 5.11 shows the sensed signals. The input voltage is around 18 V and output voltage is around 5 V in the test setup. While the voltages are closer to the actual voltages in the system, the current values measured are inconsistent.

```
Vpv: 17.77 Ipv: 0.38 Vlink: 5.40 Ilink: 1.28 Duty: 0.33
617
Vpv: 18.21 Ipv: 0.59 Vlink: 5.41 Ilink: 1.25 Duty: 0.33
613
Vpv: 18.21 Ipv: 0.36 Vlink: 5.41 Ilink: 1.24 Duty: 0.33
589
Vpv: 17.83 Ipv: 0.20 Vlink: 5.51 Ilink: 0.96 Duty: 0.33
```

Figure 5.11: Arduino serial monitor values

These inconsistencies typically arise from inconsistent sampling and any additional filtering needed. A solution would be to at first compare the current waveform with the output from the sensor, and the one read with the Arduino code considering a known fixed resistive load. This needs to be performed to properly calibrate the sensor and to further proceed with verifying the control logic, working with the solar emulator to study the charging behavior.

5.3 Challenges and Future Scope

The initial objective of the project was to develop a SIMO converter to support different load profiles. The initial study and simulation on different configurations such as cascaded buck-boost and four switch buck-boost is performed. But in the process, considering the time constraint involved and the steep learning associated with simulation and hardware design, the scope of the project was limited to design of buck converter with MPPT

implementation. The future scope on this is to design and implement a multi output converter to support multiple loads.

Also, initially the research was performed considering the target load as raw lithium ion battery, but this was replaced by the commercially purchased power bank considering the safety aspects involved. Future work could target the safety aspects involved with implementing lithium ion battery as an intermediate source powering different loads.

The decision of duty cycle step and power tolerance in P&O method involved iterative tuning to balance the tracking speed and steady state accuracy around the MPP. This could be resolved by either using an adaptive duty cycle step with respect to variation in power, or by employing a dynamic duty cycle step with duty cycle step defined based on power thresholds in the code. This would allow the system to respond faster with good accuracy under varied irradiance conditions. While the current model implementation, manages MPPT tracking with direct duty cycle control, the model could be tested with an additional inner current loop, to understand the reduction in steady state oscillations.

Though the basic functionality of the hardware PCB is tested, there are some mismatches observed in the sensed parameters and those processed and read in the Arduino. This needs to be resolved in the future to further validate the performance of the MPPT control logic implemented in Arduino.

5.4 Ethical and Social Aspects

While the proposed module utilizes renewable solar energy and the design is targeted towards outdoor recreational activities, the following ethical considerations regarding sustainability, consumer safety and operational reliability are to be considered.

- Even though the solar fed-module operates on clean renewable energy, the manufacturing of the components associated with the system structure such as the PV arrays and lithium ion batteries are resource intensive, use minerals such as lithium and cobalt. The mining process involved in such extraction can result in significant environmental degradation.

- Many consumers using this module or similar, have limited expertise and also the module is used in outdoor environments. This demands increased levels of safety precautions, to protect from risks of overheating, fire hazards etc. Future work in the project, should focus on the safety aspect of the module, in addition to the basic protection added.

- The module is targeted towards powering emergency devices such as mobile phones, power banks, GPS devices etc. It is essential to ensure no system failure occurs in these devices. Hence, a module that is reliable and does not provide a false sense of security is required.

6

Conclusion

The project successfully designed and implemented a DC-DC buck converter with MPPT. To achieve MPPT a P&O method is implemented. A MATLAB based simulation was performed to verify the MPPT and charging profile of lithium ion battery. The simulation results demonstrate the feasibility of the project and formed the basis for design and dimensioning of hardware prototype, and implementation of control logic in the Arduino.

A PCB featuring a DC-DC buck converter with sensing and protection circuits was designed using KiCad. The basic functional testing of the hardware prototype was performed validating the switching behavior and basic operation of the converter. However, there are some differences observed in the sensed parameters read in the Arduino verifying the sensor calibration, which need to be resolved to proceed with further testing of MPPT control in the hardware prototype. Once this is resolved, future testing can be performed to validate the performance of MPPT control logic.

A

MATLAB Code

The MATLAB code used in the project is shown below.

```
function [D, P] = mppt(Vpv, Ipv, State,Vb)

    if isempty(V_prev)
        V_prev = 0;
        P_prev = 0;
        D_prev = 0.5;
        integral = 0;

    end


    D_step = 0.005;
% Duty limits
    D_max = 0.95;
    D_min = 0.05;
% Compute present power
    P = Vpv * Ipv;
    % Changes
    dP = P - P_prev;
    dV = Vpv - V_prev;

    if abs(dP) > 0.01
        D_step = 0.005;
    else
        D_step = 0;
    end

%Perturb & Observe
  if (State<90)
```

```
30
31      if dP > 0
32          if dV > 0
33              D = D_prev - D_step;
34          else
35              D = D_prev + D_step;
36                      end
37      else
38          if dV > 0
39              D = D_prev + D_step;
40          else
41              D = D_prev - D_step;
42                      end
43      end
44
45  %PI regulator
46    else
47        Vref = 4.2;
48        error = Vref - Vb;
49      Kp = 0.1;
50      Ki = 5;
51      Ts = 20e-3;
52  Prop = Kp*error;
53  Integralsum  = integral + (error*Ts);
54  Int = Ki*Integralsum;
55  Ctrlduty = Prop + Int;
56
57  % Anti windup
58          if(((Ctrlduty<= D_max)&&(Ctrlduty >=D_min))||(sign(error)
                ~=sign(Ctrlduty)))
59          integral =Integralsum;
60          end
61
62  % Saturation
63  D = max(D_min, min(D_max,Ctrlduty));
64    end
65
66  if (D>D_max)
67      D = D_max;
68  else
69      if(D<D_min)
```

```
70          D= D_min;
71      end
72  % Update stored values
73      V_prev = Vpv;
74      P_prev = P;
75      D_prev = D;
76  end
```

Listing A.1: MATLAB Implementation Code

B

Arduino IDE Code

The Arduino IDE code used in the project is shown below.

```
// PIN SETUP
const int DC_LINK_VOLT   = A0;
const int DC_LINK_CURR   = A1;
const int PV_CURRENT_IC  = A2;
const int PV_VOLTAGE_PIN = A3;
const int PV_CURRENT_RES = A4;
const int PWM_PIN        = 11;




// SENSOR CALIBRATION
float PV_voltageScale = 6;
float LINK_voltageScale = 3.3256;

float currentOffset = 2.5;
float currentScale  = 0.4;

// CONTROL VARIABLES
float Vp = 0;
float Pp = 0;
float Dp = 0.5;
float Change = 0.001;
bool initialized = false;

// TIMING
unsigned long lastTime = 0;
const unsigned long Ts_us = 50000;


```

```
30 void setup() {
31
32  pinMode(11,OUTPUT);
33   TCCR1A = 0;
34   TCCR1B = 0;
35
36 // Fast PWM, TOP = ICR1
37   TCCR1A |= (1 << COM1A1);           // PWM on pin 11
38   TCCR1A |= (1 << WGM11);
39   TCCR1B |= (1 << WGM12) | (1 << WGM13);
40
41   TCCR1B |= (1 << CS10);             // prescaler = 1
42
43   ICR1 = 319;                        // 50 kHz
44   Serial.begin(115200);
45 }
46
47 // VOLTAGE AND CURRENT READING
48 float readVoltage(int pin) {
49   int raw = analogRead(pin);
50   float voltage = (raw / 1023.0) * 5.0;
51
52   if (pin == DC_LINK_VOLT){
53     return voltage * LINK_voltageScale;
54   }
55   else {
56     return voltage * PV_voltageScale;
57   }
58 }
59
60 float readCurrent(int pin) {
61   int raw = analogRead(pin);
62   float voltage = (raw / 1023.0) * 5.0;
63   return (voltage - currentOffset) / currentScale;
64 }
65
66 // MPPT
67 float computeDuty(float V, float I) {
68
69   if (!initialized) {
70     Vp = V;
```

```
71      Pp = V * I;
72      Dp = 0.3;
73      initialized = true;
74    }
75
76    float P = V * I;
77    float D;
78
79    if (P > 9.7 && P < 10.3) {
80      Change = 0.0001;
81    } else {
82      Change = 0.001;
83    }
84
85    if (P > Pp) {
86      if (V > Vp) D = Dp - Change;
87      else        D = Dp + Change;
88    } else {
89      if (V > Vp) D = Dp + Change;
90      else        D = Dp - Change;
91    }
92
93    if (D > 0.8) D = 0.8;
94    if (D < 0.2) D = 0.2;
95
96    Vp = V;
97    Pp = P;
98    Dp = D;
99
100   return D;
101 }
102
103 int printCounter = 0;
104
105 void loop() {
106
107   unsigned long now = micros();
108
109   if (now - lastTime >= Ts_us) {
110     lastTime = now;
111
```

```
112     float Vpv  = readVoltage(PV_VOLTAGE_PIN);
113     float Ipv  = readCurrent(PV_CURRENT_IC);
114     float Vout = readVoltage(DC_LINK_VOLT);
115     float Ilink = readCurrent(DC_LINK_CURR);
116 
117     float duty = computeDuty(Vpv, Ipv);
118 
119     OCR1A = duty*319;
120 
121 
122 // PRINTING BLOCK
123     printCounter++;
124     if (printCounter >= 10) {  // every ~500 ms
125       printCounter = 0;
126       Serial.println(analogRead(DC_LINK_CURR));
127       Serial.print("Vpv: "); Serial.print(Vpv);
128       Serial.print(" Ipv: "); Serial.print(Ipv);
129       Serial.print(" Vlink: "); Serial.print(Vout);
130       Serial.print(" Ilink: "); Serial.print(Ilink);
131 
132       Serial.print(" Duty: "); Serial.println(duty);
133     }
134   }
135 }
```

References

[1] A. Murphy, "New survey confirms popularity of hiking, surfing, skiing, camping, and other outdoor activities continues to boom," *Outdoors*. [Online]. Jan. 3, 2024. Accessed on: 2026-05-07

[2] European Commission, Eurostat, "Nature calling: interest in camping & caravanning grows" 2026 [Online]. Accessed on: 2026-05-07.

[3] O. M. Toledo, D. de Oliveira Filho, and A. S. A. C. Diniz, "Distributed photovoltaic generation and energy storage systems: A review," Renewable and Sustainable Energy Reviews, vol. 14, no. 1, pp. 506–511, Jan. 2010, doi:10.1016/j.rser.2009.08.007.

[4] R.L. San Martin, "Solar energy", AccessScience, Nov. 2025, doi:10.1036/1097-8542.633300

[5] M. Seyedmahmoudian et al, "Simulation and Hardware Implementation of New Maximum Power Point Tracking Technique for Partially Shaded PV System Using Hybrid DEPSO Method," IEEE Transactions on Sustainable Energy, vol. 6, no. 3, pp. 850-862, July 2015, doi:10.1109/TSTE.2015.2413359.

[6] W.K. Fox, "Energy source", AccessScience, Nov. 2025, doi:10.1036/1097-8542.233000

[7] X. Li et al, “Review and perspective of materials for flexible solar cells,” Materials Reports: Energy, vol. 1, no. 1, Feb. 2021, doi:10.1016/j.matre.2020.09.001.

[8] S. K. Mahapatro, "Maximum Power Point Tracking (MPPT) Of Solar Cell Using Buck-Boost Converter", INTERNATIONAL JOURNAL OF ENGINEERING RESEARCH & TECHNOLOGY (IJERT) Vol. 2, no. 5, May. 2013, doi:10.17577/IJERTV2IS50323.

[9] W. Shen, T. T. Vo, and A. Kapoor, “Charging algorithms of lithium-ion batteries: An overview,” in 7th IEEE Conference on Industrial Electronics and Applications (ICIEA), Singapore, 2012, pp. 1567-1572, [Online], Accessed on date: 2026-02-24

[10] C. I. Idu, U. O. Uyor, A. P. I. Popoola, O. M. Popoola, and S. M. Adams, “A review of recent advances, current limitations, and remedies of lithium-ion batteries for advanced technological applications,” Future Batteries, vol. 7, Sep. 2025, doi:10.1016/j.fub.2025.100109.

[11] M.-K. Tran and M. Fowler, “A review of lithium-ion battery fault diagnostic algorithms: Current progress and future challenges,” Algorithms, vol. 13, no. 3, Mar. 2020, doi:10.3390/a13030062.

[12] O. S. H. Saleh, K. S. H. Saleh, and I. I. Abdallah, “An Overview on Photovoltaic System,” iRASD Journal of Energy & Environment, vol. 5, no. 2, pp. 76–100, Dec. 2024, doi:https://doi.org/10.52131/jee.2024.0502.0046.

[13] M. H. Ali, M. Zakaria, and S. El-Tawab, “A comprehensive study of recent maximum power point tracking techniques for photovoltaic systems,” Scientific Reports, vol. 15, art. no. 14269, Apr. 2025. [Online], doi:10.1038/s41598-025-96247-5

[14] D. Verma, S. Nema and R. K. Nema, "Implementation of perturb and observe method of maximum power point tracking in SIMSCAPE/MATLAB," in 2017 International Conference on Intelligent Sustainable Systems (ICISS), Palladam, India, 2017, pp. 148-152, [Online], Accessed: 2026-02-26

[15] N. Mohan, T. M. Undeland, W. P. Robbins, "dc-dc SWITCH MODE CONVERTERS" in *Power Electronics: Converters, applications and design*, 3rd ed, B. Zobrist, Ed. Hoboken, NJ, USA: John Wiley and sons, inc, 2003, pp 161-199.

[16] M. Zhao, D. Zhang, Z. Zhou, T. Li and Z. Wang, "Novel method for failure prognostics of power MOSFET," 2015 IEEE International Conference on Computational Intelligence and Virtual Environments for Measurement Systems and Applications (CIVEMSA), Shenzhen, China, 2015, pp. 1-4, [Online], Accessed: 2026-04-10

[17] Y. Gao, A. Q. Huang, S. Krishnaswami, J. Richmond and A. K. Agarwal, "Comparison of Static and Switching Characteristics of 1200 V 4H-SiC BJT and 1200 V Si-IGBT," in IEEE Transactions on Industry Applications, vol. 44, no. 3, pp. 887-893, May. 2008, doi: 10.1109/TIA.2008.921408.

[18] Newcomb, R.W. "Circuit (electronics)", AccessScience, Nov. 2025, doi: 10.1036/1097-8542.137000.

[19] K.J. Hintz, "Programmable controller", AccessScience, Jan. 2026, doi:10.1036/1097-8542.547500

[20] Arduino, "What is Arduino?", 2022, [Online]. Accessed: 2026-04-28).

[21] A. T. Bryant, Y. Wang, S. J. Finney, T. C. Lim, and P. R. Palmer, “Numerical optimization of an active voltage controller for high-power IGBT converters,” IEEE Transactions on Power Electronics, vol. 22, no. 2, pp. 374–383, Mar. 2007, doi: 10.1109/TPEL.2006.890009.

[22] S. K. Sahoo, A. Ramulu, S. Batta and S. Duggal, "Performance analysis and simulation of three phase voltage source inverter using basic PWM techniques," in IET Chennai 3rd International on Sustainable Energy and Intelligent Systems (SEISCON 2012), Tiruchengode, India, 2012, pp. 1-7, Accessed: 2026-04-20

[23] P. Sun, C. -L. Chen, J. -S. Lai and C. Liu, "Cascade dual-buck full-bridge inverter with hybrid PWM technique," 2012 Twenty-Seventh Annual IEEE Applied Power Electronics Conference and Exposition (APEC), Orlando, FL, USA, 2012, pp. 113-119, Accessed: 2026-04-20

[24] B. Hauke, "Basic Calculation of a Buck Converter’s Power stage" Texas Instruments, Dallas, USA, SLVA477B, Dec 2015. [Online]. Accessed: 2026-04-27.

[25] “USB 2.0 Specification”, usb_20.pdf, ch. 3.1 "Goals for the Universal Serial Bus, USB-IF, Mar. 2025, accessed May 06, 2026.

[26] “Battery Charging v1.2 Spec and Adopters Agreement”, BC1.2 plus errata 2012-3-15.pdf, ch. 1.4.7 "Dedicated Charging Port", USB-IF, Nov. 2019, accessed May 06, 2026.

[27] Dr.F.Golnaraghi and Dr.B.C.Kuo, "Design of control systems", *Automatic control systems*, 10th edition, chapter 11.1-11.2, Accessed: 2026-04-22

[28] *Datasheet - PSM-12V-10W*, RS components, SEEIT, Accessed: 2026-03-10

[29] *1400 Series — Bobbin Type Inductors*, Westborough, USA: Murata Power Solutions, Inc, 2018. [Online]. Accessed: 2026-04-02

[30] *30V N-Channel MOSFET*, Sunnyvale, USA: ALPHA & OMEGA SEMICONDUCTORS, 2023. [Online]. Accessed: 2026-04-01

[31] M. Xie, "How to select input capacitors for a buck converter" Texas Instruments, Dallas, USA, SLYT670, 2016, Accessed: 2026-04-29.

[32] *High Power Density 1.2A Boost Regulator*, San Jose, USA: MICREL, INC, JAN 2010, [Online], Accessed: 2026-03-20

[33] *NEBO 10K POWER BANK*, Roanoke, USA: Alliance Sports Group, L.P., 2025. [Online], Accessed: 2026-03-12

[34] *High Accuracy, Galvanically Isolated Current Sensor IC With Small Footprint SOIC8 Package*, Worcester, USA: Allegro MicroSystems, Jun. 2014. [Online], Accessed: 2026-03-16

[35] L.E.Frenzel, Jr, "Voltage Dividers", in Practical Electronic Design for Experimenters, 1st Edition, chapter 5.3, Accessed: 2026-04-20

[36] *Automotive P-Channel 20 V (D-S) 175 °C MOSFET*, Malvern, USA: VISHAY INTERTECHNOLOGY, INC, 2025. [Online]. Accessed: 2026-04-02

[37] O. Ibrahim, N. Z. Yahaya, N. Saad and M. W. Umar, "MATLAB/Simulink model of solar PV array with perturb and observe MPPT for maximising PV array efficiency," in 2015 IEEE Conference on Energy Conversion (CENCON), Johor Bahru, Malaysia, 2015, pp. 254-258, [Online], Accessed: 2026-03-27.

[38] Adrian, “Easy PCB Trace Width Calculation: A Step by Step Guide for Hobbyists,” *AllElectroHub*. [Online]. Sep. 2025, Accessed: 2026-04-23